Observations of sunlit N_2^+ aurora at high altitudes during the RENU2 flight

Pål Gunnar Ellingsen[1], Dag Lorentzen[2,3], David Kenward[4], James H Hecht[5], J. Scott Evans[6], Fred Sigernes[2,3], and Marc Lessard[4]

[1] Department of Electrical Engineering, UiT The Arctic University of Norway, 8505 Narvik, Norway
[2] Department of Arctic Geophysics, the University Centre in Svalbard, P.O. Box 156, 9171 Longyearbyen, Norway
[3] Birkeland Centre for Space Science, Department of Physics and Technology, University of Bergen, 5020 Bergen, Norway
[4] The University of New Hampshire, Durham, NH 03824, USA
[5] Space Science Applications Laboratory, The Aerospace Corporation, El Segundo CA, USA
[6] Computational Physics Inc., Springfield, VA, USA

Correspondence: Pål Gunnar Ellingsen (pal.g.ellingsen@uit.no)

Abstract. We present measurements of sunlit aurora during the launch of the Rocket Experiment for Neutral Upwelling 2 (RENU2) on the 13 December 2015, 07:34 UTC. The *in situ* auroral conditions coincide with those of sunlit aurora, and were characterised by the 391.4 nm and 427.8 nm N_2^+ emissions. A correlation between several auroral wavelengths, as measured by a meridian scanning photometer was used to detect sunlit aurora and indirectly neutral upwelling. These results, based on ground data, agree well with the RENU2 measurements recorded during its pass through the sunlit polar cusp. Using *in situ* data from RENU2 and the solar photon flux, it was estimated that sunlit aurora was a major part ($\approx 40\%$) of the observed 427.8 nm emission.

1 Introduction

Upwelling of neutrals and ions is known to occur in the cusp region of the auroral oval (Lühr et al., 2004; Lorentzen et al., 2007; Carlson et al., 2012; Sadler et al., 2012). The upwelling is known to significantly increase the density of the upper ionosphere, and can be observed by proxy as an increase in satellite drag over the cusp (Lühr et al., 2004). The underlying mechanisms behind the increased density above 400 km are not fully understood, and several explanations have been proposed. Carlson et al. (2012) used a first-principle physics model to show an increase in cusp and polar cap densities due to plasma flow shear through soft electron precipitation. According to a theoretical study by Deng et al. (2013), the precipitation of soft electrons together with a Poynting flux contributed to an increase in neutral density at 400 km. The electrons contributed to an increase in the Pedersen conductivity in the F-region. Electrons with around 100 eV of energy dominated this process. Cohen et al. (2015) used a model to study the relation between electron temperature and density, and ion upwelling. They found that auroral precipitation, electron temperature and density increases all result in an increased upwelling. Due to the localised nature of the upwelling and lack of good techniques for remote measurement of neutrals in the ionosphere, sounding rockets have been used to gather *in situ* observations.
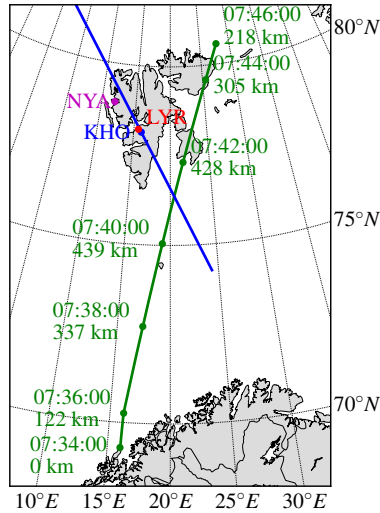
Figure 1. Figure showing the ground track for the RENU2 rocket, green, and the Meridian Scanning Photometer (MSP) scan line, blue, when scanning above $20°$ elevation angle. The location of Longyearbyen (LYR), Ny-Ålesund (NYA) and the Kjell Henriksen Observatory (KHO) are shown.

The Rocket Experiment for Neutral Upwelling 2 (RENU2) was launched from Andøya Space Centre (ASC) on the 13 December 2015, 07:34 UTC ($\approx$10:34 MLT). It flew through a sun illuminated cusp over Eastern Svalbard. The launch track is shown Figure 1. The payload carried a large variety of instruments for measuring the *in situ* magnetic and electric fields, ion and electron density and energy, optical emissions and more. Details about the sounding rocket and its instrumentation can be found in the overview article for RENU2 (Lessard et al., 2019).

During the RENU2 campaign ground-based support was available from Svalbard, both from Longyearbyen (LYR) and Ny-Ålesund (NYA), see figure 1. Support from the SuperDARN network of HF radars was also given (Greenwald et al., 1995; Chisham et al., 2007). In addition to collecting data for post-launch analysis, data was used as input for the launch decision. In this paper we will concentrate on optical ground-based data from LYR site, the Kjell Henriksen Observatory (KHO, Geographical coordinates: N $78.148°$, E $16.043°$, magnetic coordinates (2015): N $75.55°$, E $109.66°$) in combination with rocket data, and focus will be studying the link between sunlit aurora and neutral upwelling, and how different processes contribute to the N_2^+ emissions.

2 Theory

2.1 Nitrogen ionisation and emission

Cusp aurora is optically characterised by an irradiance ratio I(630.0nm/557.7nm) > 1, and a typical electron precipitation energy of ≈ 0.5 keV. The Kjell Henriksen Observatory is placed directly beneath the statistical dayside auroral oval, with a

negative solar zenith angle for more than two months of the year. However, parts of the ionosphere will always be sunlit in the daytime. The cusp auroral red emission line - 630.0 nm [OI] - has an average emission altitude of ≈ 250 km (Johnsen et al., 2012) due to collisional quenching at lower altitudes. In addition to the atomic oxygen emission, emissions in the first negative

40 band of the N_2^+ ions have previously been observed in the sunlit part of the ionosphere at Svalbard (Deehr et al., 1980). During the RENU2 launch, the onboard photometer observed the 391.4 nm N_2^+ 1N (0,0) emission, while the ground based Meridian Scanning Photometer at KHO observed the 427.8 nm N_2^+ 1N (0,1) emission.

The ionised nitrogen in the auroral N_2^+ 1N band is normally produced by direct ionisation via electron impact

$$N_2 + e \longrightarrow N_2^+ + e + e^{'}$$
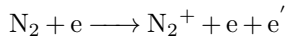
45 where $e^{'}$ is a thermal electron.

However ionised nitrogen can also be produced from molecular nitrogen by solar extreme ultra violet (EUV) radiation via (Hunten, 2003; Jokiaho, 2009)

$$N_2 + h\nu(< 79.6 \ nm) \longrightarrow N_2^+ + e,$$
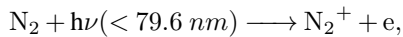
where $h\nu$ is the EUV photon.

50 Under sunlit conditions in the ionosphere, the N_2^+ ion in its ground state (X), can experience resonant absorption of solar photons, ending up in an excited state (N_2^+ A or B) and thus contributing to emissions from the Meinel or 1N band, respectively. The more common way of exciting N_2^+ is through precipitating electrons. In sunlit aurora it is expected that both will occur, while in non sunlit condition, only precipitating electrons will excite the N_2^+.

2.2 EUV illumination of the ionosphere

55 At the time of the rocket launch, the area North of the launch site (ASC) was experiencing polar night, with the Sun continuously below the horizon, as seen from the ground. Higher altitudes had some sunlight, though the amount of EUV radiation depends on what part of the atmosphere the solar radiation had propagated through (Cohen et al., 2015). The penetration depth of EUV is wavelength dependent, and the majority of the EUV spectrum is attenuated by at least $1/e$ below 150 km (Brasseur, 1986). Therefore we will define a sunlit ionosphere as an ionosphere where the incident EUV has not propagated lower than 150 km

60 before reaching the point of interest.

In this article the definition of sunlit aurora will be the same as the one by Hunten (Hunten, 2003). In this summary he specifies that sunlit aurora occurs when N_2^+ fluoresces in the blue and violet as a result of being excited from the ground state by higher energy sunlight.

2.3 Poleward moving auroral forms and cusp processes

65 It is known from literature that Poleward moving auroral forms (PMAFs) are associated with cusp aurora processes such as neutral and ion upflows (Moen et al., 2004), polar cap patches (Lorentzen et al., 2010) and flow channels (Sandholt and Farrugia, 2007; Herlingshaw et al., 2019). PMAFs are ionospheric signatures of pulsed magnetopause reconnection (Fasel,

1995; Sandholt and Farrugia, 2007). The upflows present under PMAFs can allow for the generation of sunlit aurora due to the increased availability of nitrogen at higher altitudes. If the ionosphere is illuminated by solar EUV (subsection 2.1), nitrogen can be ionised, making it available for resonant scattering of sunlight. This gives rise to one of the more commonly studied sunlit aurora bands, the first negative band of N_2^+, and then especially its emission at 427.8 nm (Chakrabarti, 1998; Hunten, 2003).

3 Observations

The ground based optical observations were done under partly overcast conditions, with some light snow in the air. These observations were done with several types of optical instruments, but in this work we will concentrate on the meridian scanning photometer (MSP), and a $180°$ fisheye all-sky camera. From the RENU2 payload, measurements from the electron plasma sensor (EPLAS) and the three photometers will be utilised. Measurements of incident EUV were acquired from the EVE experiment on the Solar Dynamics Observatory satellite. Using the OMNI solar wind data service, it was seen that the interplanetary magnetic field component, B_z, turned southward at about 06:00 UTC, and stayed negative until about 13:00 UTC, with a weakly negative value of -1.5 nT throughout the time period.

3.1 Meridian scanning photometer

The Meridian Scanning Photometer (MSP) scans the magnetic meridian, see figure 1, at three different wavelengths; 630.0 nm, 557.7 nm and 427.8 nm. The two first wavelengths are OI lines, while the last is the previously mentioned N_2^+ line. Narrow interference filters, with a bandpass of ≈ 0.4 nm, are mounted in individual tilting filter holders. By tilting the filter away from the measured emission line, the background can be measured and subsequently subtracted. Each revolution of the scanning mirror takes 4 s. One background subtracted scan consequently takes 8 s. Two of these background subtracted scans are averaged to give a complete acquisition time of 16 s.

Figure 2 shows 3 hours of MSP data centered around the time of launch (07:34 UTC). Prior to the launch a number of poleward moving auroral forms (PMAFs) are observed. The first ones are seen around 06:30 UTC. PMAFs are indicative of pulsed magnetopause reconnection (i.e flux transfer events) (Sandholt and Farrugia, 2007; Russell and Elphic, 1978). The payload flew East of KHO, and through the extended PMAF located on the keogram between 07:40 UTC (360 s) and 07:45 UTC (540 s) and 120 to 60 degrees scan angle.

3.2 All-sky camera

The all-sky camera in use during the rocket campaign was a Sony a7s equipped with a 180 degree fisheye lens (Sigma 8mm f/3.5 EX DG Circular Fisheye). It is a full format CMOS camera, and was taking images every 30 s with a 5 s exposure. During the launch there was light snow settling on the dome of the camera (cleaned periodically). The images collected were sufficient to see that during the launch there was a clear arc of dayside aurora overhead, extending from magnetic east to magnetic west. A video (Sony_launch.mp4) of these images can be found in the supplemented material.
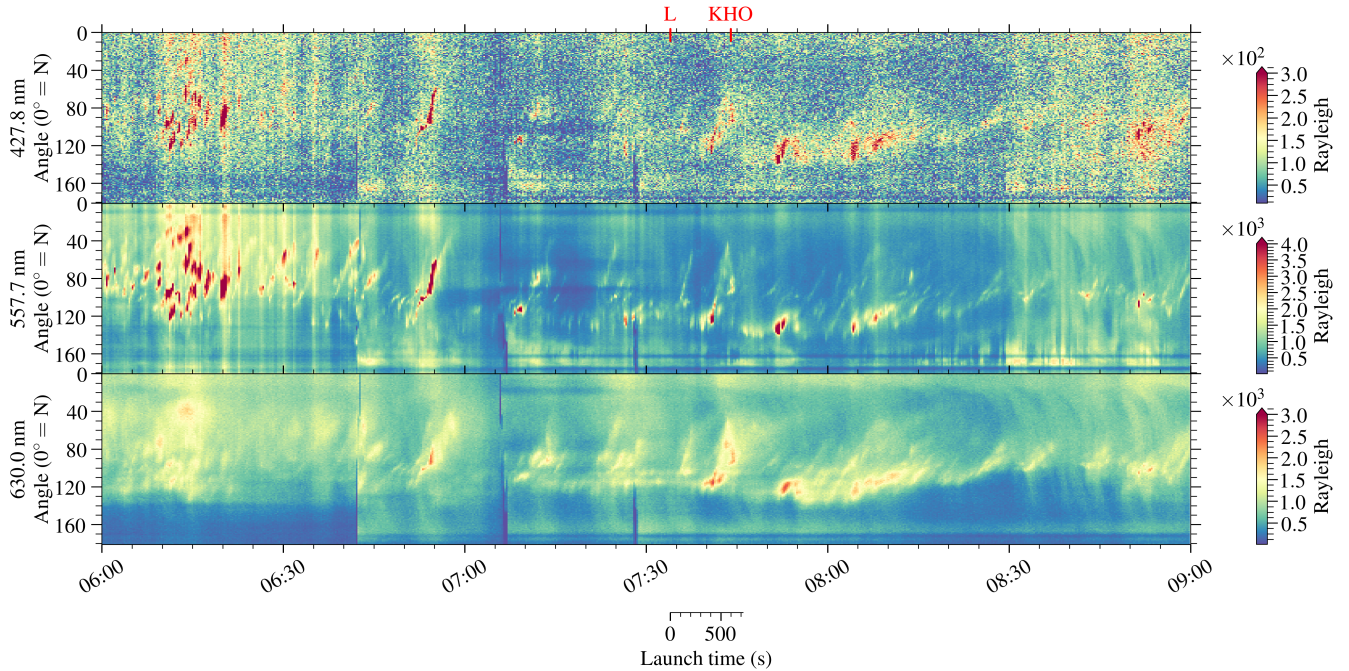
Figure 2. The MSP data from 6 UTC to 9 UTC. It shows the three recorded wavelengths over the North to South scan along the magnetic meridian. The vertical dark blue stripes are from when the slit covering the MSP was cleaned of snow. *L* and *KHO* mark the launch and passing east of KHO.

3.3 RENU2 photometers

100 RENU2 was equipped with a three-channel photometer measuring the red 630.0 nm OI emission, the green 557.7 nm OI emission and the 391.4 nm N_2^+ 1N (0,0) emission. Details of the instrumentation can be found in (Lessard et al., 2019). In this work, the focus will be on the nitrogen channel. Observations and analysis from the other two channels are available in the paper by Hecht et al. (2019).

3.4 RENU2 Electron Plasma Sensor and EVE Solar Dynamics Observatory

105 In this work, we utilize two instruments; the Electron Plasma Sensor (EPLAS) detector onboard the RENU2 rocket and the Extreme Ultraviolet Variability Experiment (EVE) onboard the Solar Dynamics Observatory (SDO) satellite (Pesnell et al., 2012). EVE contains two spectrographs; MEGS-A (6–33 nm) and MEGS-B (33–105 nm). Unfortunately MEGS-A broke on the 26 May 2014, leaving only MEGS-B working. In figure 3 the average irradiance on the day of the rocket (dashed orange), in addition to the closest day when the MEGS-A was running (blue line) can be seen. The closest match was calculated by
110 correlating the valid parts of the spectra together. In the figure the spectral lines which are part of the solar EUV spectrum can be seen on top of a dimmer continuous spectrum.
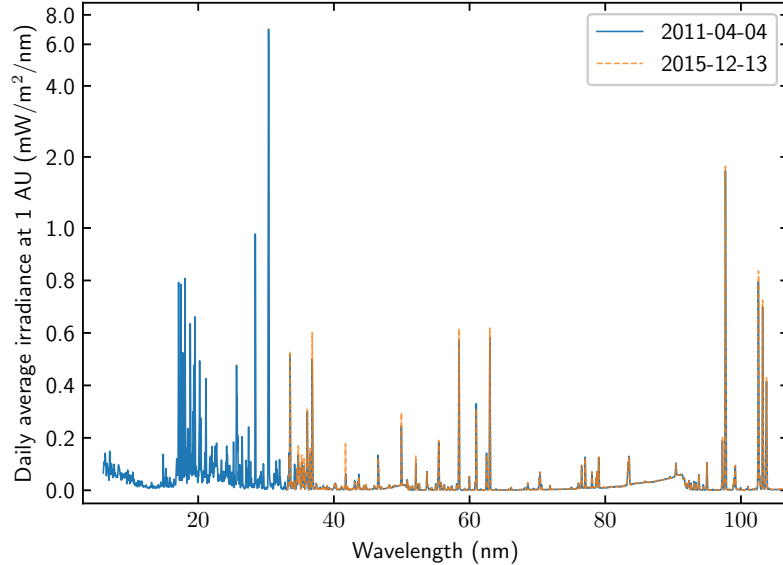
Figure 3. Measurements of daily average irradiance at 1 AU from the EVE instrument from the day of the launch 13 December 2015 (orange) and the closest match to the launch day from when the MEGS-A detector worked (blue). Notice that the irradiance scale is linear below 1 mW/m^2/nm and logarithmic above.

The Electron Plasma (EPLAS) instrument is a tophat electrostatic analyzer which measures electron energy from 5 eV to 14.6 keV around a 360 degree field of view with 10 degree pitch angle resolution and 42 ms time resolution. The energy steps are logarithmic, and each step has 1 ms dwell time. Further details can be found in Kenward et al. (2019). Figure 4 shows the measurements taken when the rocket passed through the cusp. In the left plot the characteristic energies of the electrons can be seen. The values are above 50 eV for the whole duration, with some short bursts reaching energies above 200 eV. In the right plot the electron flux is shown. It shows a significant increase in flux at 550 s (07:44:10 UTC) which subsides again at 630 s (07:45:30 UTC). The increase is not constant within this time period, but comes in both shorter and longer bursts.

4 Analysis and discussion

4.1 Auroral measurements in sunlit aurora

We will now investigate if the ground based 428.7 nm N$_2^+$ emissions observed during the sounding rocket launch can be classified as sunlit aurora, and if the ionisation is driven by solar EUV or precipitating electrons. In order to find the contribution of the different processes, we first start by looking at the ionisation rates. Calculating these rates requires knowledge of the amount of EUV flux at a given height and the particle flux of precipitating electrons. RENU2 reached the Svalbard latitudes
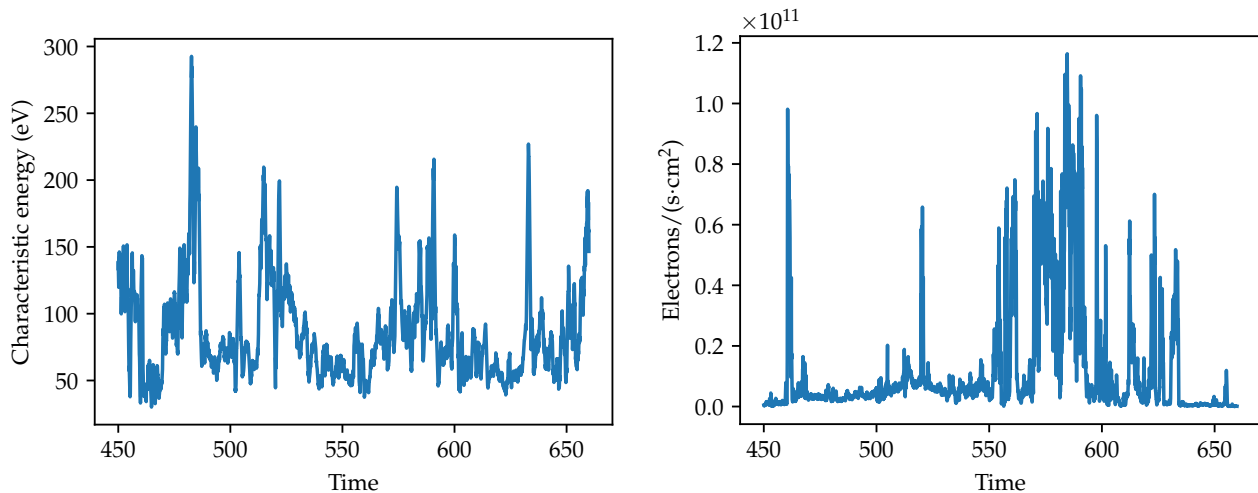
Figure 4. EPLAS characteristic energies (left) and electron flux (right) for the part of the flight where the rocket was in the cusp. The x-axis is in flight time with 450 s corresponding to 07:41:30 UTC and 650 s to 07:44:50 UTC. For a more detailed data set, see Kenward et al. (2019).

at around 07:41 UTC (420 s) on the 13 December 2015. At that time the solar depression angle was 15 degrees, and the ionosphere was sunlit above ≈ 223 km altitude (per definition in subsection 2.2). The sounding rocket was, at that time, close to its apogee altitude of ≈ 450 km, and thus well within the sunlit part of the ionosphere.

4.1.1 EUV photon flux

The EUV flux incident on atmosphere can be obtained from the Extreme Ultraviolet Variability Experiment (EVE) (Woods et al., 2012; Hock et al., 2012; Didkovsky et al., 2012) on the Solar Dynamic Observatory (SDO) satellite (Pesnell et al., 2012). Using the Level 3 daily average irradiance data (downloaded in 2017), it is possible to calculate the total irradiance in the wavelength range 33–79.6 nm at 1 AU. On the 13 December 2015, (see figure 3) it is found to be 0.83 mW/m^2. After 2014, only the MEGS-B instrument on the SDO EVE platform - which detects wavelengths above 33 nm - was working. Prior to its failure in 2014, the MEGS-A measured between 6–33 nm. As there are some strong spectral lines below 33 nm, a calculation of the irradiance needs to include the region down to 6.0 nm. In order to extrapolate the incoming EUV irradiance to the original measurement region, the complete merged Level 3 data from the EVE instrument over the total spectrum from 6.0 nm to 79.8 nm was averaged over the complete time series for the instrument (2010–2017). Thus, by comparing the regions below and above 33 nm with the total average, it was found that the total irradiance for the full wavelength range of 6.0–79.8 nm is $\approx 4\times$ the irradiance above 33 nm, with a standard deviation of 1. To check this factor the spectrum closest to the one on the 13th was found by correlating the valid parts (33–79.6 nm) of the spectrum with the daily averages from before the MEGS-A broke. The highest correlation was found with 4 April 2011, shown in figure 3, with a correlation coefficient of 0.9937. This

spectrum had a factor of 4.03. Taking both approaches into account, a factor of 4 for the time of the RENU2 launch will be used, yielding a total EUV irradiance of 3.3 mW/m^2 at a distance of 1 AU.

By using the calculated EUV irradiance, the photon flux can be found using:

$$j_\gamma = \frac{I}{E_\gamma} = \frac{I\lambda}{hc} \tag{1}$$

where I is the irradiance, E_γ the photon energy, λ the wavelength, h the Planck constant and c the speed of light. To get an estimate, we can set $\lambda = 50$ nm based on the invariability of the photoionisation cross section from approximately 30 nm to 70 nm (Itikawa et al., 1986) and use the calculated irradiance $I = 3.3$ mW/m^2 to get $j_\gamma \approx 8.3 \cdot 10^{10}$ cm^{-2}s^{-1}.

4.1.2 Electron flux

The particle flux of precipitating electrons can be obtained using the Electron Plasma Sensor (EPLAS) on the RENU2 payload, for more details see (Lessard et al., 2019; Kenward et al., 2019). EPLAS measured electron energy, flux and pitch angles for electrons with energy between 10 eV and 15 keV. From the measurements shown in figure 4 the average electron flux was found to be $j_e \approx 1.2 \cdot 10^{10}$ cm^{-2}s^{-1} in the time period between 07:41:30 UTC (450 s) and 07:44:50 UTC (650 s) when the rocket was in the cusp. The characteristic energy for these electrons were between from 50 eV to over 100 eV (with peaks of up to 300 eV).

4.1.3 Ionisation rates

The last parameters needed to calculate the ionisation rates, are the cross sections for ionisation of N$_2$. From literature it is found that the photoionisation cross section for N$_2$ is $\sigma_\gamma \approx 2 \cdot 10^{-17}$ cm^2 (Itikawa et al., 1986). The electron impact ionisation cross sections on N$_2$ in the range around 100 eV is $\sigma_e \approx 2 \cdot 10^{-16}$ cm^2 (Bug et al., 2013; Tabata et al., 2006). Using these together with the photon and electron fluxes found in the previous subsections, the photoionisation rate is found to be

$$q_\gamma = j_\gamma \cdot \sigma_\gamma = 1.7 \cdot 10^{-6} \text{ s}^{-1}, \tag{2}$$

while the electron ionisation rate is found to be

$$q_e = j_e \cdot \sigma_e = 2.4 \cdot 10^{-6} \text{ s}^{-1}. \tag{3}$$

These numbers indicate that the EUV can contribute up to 40% of the total production of N$_2{}^+$ at the time of measurement, assuming steady state conditions where there is enough N$_2$ available for ionisation. The two rates being comparable (within the limits of the estimate given above), means that in solar EUV conditions one should be careful in classifying EUV as the only production mechanism for N$_2{}^+$, as an increase in the precipitating electrons can drive the production of N$_2{}^+$ as well. Some of the produced N$_2{}^+$ is already in an excited state, as the cross section for photoionisation into the B$^2\Sigma_u{}^+$ state, is $\approx 2 \cdot 10^{-17}$ cm^2 for photons with wavelengths in the 50 nm region (Itikawa et al., 1986). The corresponding cross section for electrons at 100 eV is $\approx 5 \cdot 10^{-18}$ cm^2 (Itikawa et al., 1986). These estimated rates are only a small part of the complicated photochemistry of N$_2{}^+$ (Abdou et al., 1984).

When observing from the ground, one observes the N_2^+ ions via the 427.8 nm emission, excited by electrons. One would then also be measuring light from for instance resonant scattering of sunlight. Remick et al. (2001) estimated the enhancement from resonant scattering at $\approx 50\%$ compared to non sunlit conditions, but these estimates could include water absorption, Rayleigh scattering and other uncertainties. Similarly Jokiaho et al. (2009) used remote sensing data in combination with a steady state model and found that a more comprehensible model is needed for a complete understanding. This together with the difference in the scanning direction of the MSP and the rocket path of the RENU2 rocket, see figure 1, means that no direct comparison between the estimate and the observed 427.8 nm will be done.

4.1.4 Availability of N_2

In the previous section we estimated the ionisation rates of N_2 through two different processes. These rates require there to be enough N_2 available at the point of ionisation. Determining the amount of available N_2 at a given altitude is challenging, especially in the cusp. A baseline can be found using the NRLMSISE-00 atmospheric model for the location and time of interest. If we input the location above KHO and time of the launch, the model returns the profiles shown in figure 5. These model results show that the concentration of molecular nitrogen above 400 km is at least two orders of magnitudes smaller than that of atomic oxygen. As mentioned the model is not correct in the cusp, as there is an increase in the density of neutrals
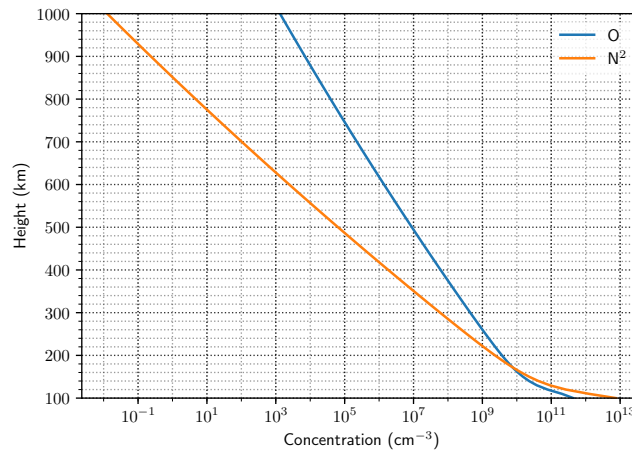
Figure 5. An NRLMSISE model of the nitrogen and atomic oxygen content above the KHO observatory in Longyearbyen for the time of the launch (UTC 7.5). From the ccmc modelweb, *https://ccmc.gsfc.nasa.gov/modelweb/models/nrlmsise00.php*, M. Picone, A.E. Hedin and D. Drob, Naval Research Laboratory. (Picone et al., 2002).

at these higher altitudes, due to heating and ion upflow (Carlson et al., 2012; Sadler et al., 2012; Lessard et al., 2019). Such an increase provides a significant amount of available neutral nitrogen for ionisation. Under these conditions the model predictions can be viewed as a lower bound for the conditions.

4.1.5 Auroral observations from the RENU2 photometers

190 Hecht et al. (2019) report observations from the redline and greenline photometers onboard the RENU2 rocket. These data are accompanied by a model which includes dayglow and auroral precipitation, the latter based on the onboard electron spectrometer data. Also onboard RENU2 was a third photometer that measured emission from the (0,0) band of the N_2^+ 1NG system at 391.4 nm (blue emission) that arises from direct electron precipitation and resonance scattering from sunlit N_2^+ ions that are produced by the precipitation (Romick et al., 1999). In the absence of precipitation dayglow emission is observed from

195 resonance scattering from ambient N_2^+ ions produced by solar photons or photoelectrons but this is a minor portion of the observed emission. The field of view of the photometers was 3.2 degree and the instrument was pointed in the zenith although the rocket spun and some glint was observed as described in Hecht et al. (2019). The photometer bandpass was narrow enough, at about 3 nm full-width at half maximum, to isolate the (0,0) band.

To model the data two long-established models were used to predict the emissions that could be observed during the flight.

200 AURIC (Strickland et al., 1999) modelled the dayglow emissions and B3C (Strickland et al., 1993) modelled the auroral emissions. The input to the B3C model, as noted in Hecht et al. (2019), included an onboard electron spectrometer that identified auroral precipitation events. The resonant scattering of sunlight off background N_2^+ ions was predicted by the models to dominate the emission for most of the flight prior to about 450 seconds. After that time until about 630 seconds the modeling predicted that the observed 391.4 nm emission, above the rocket, would be enhanced due to the auroral precipitation that the

205 rocket passed through. However, during this period the AURIC/B3C modeling shows, for emissions above the rocket, that the resonance scattering component of the 391.4 nm emission, that is enhanced due to the increased production of N_2^+ ions during an auroral precipitation event, vastly exceeds the direct auroral emission component.

Figure 6 shows the RENU2 results where the model data is in the same format as in Hecht et al. (2019). Note that the model is not adjusted for any composition changes although it does account for the portion of the blue emission due to ion production

210 during precipitation and the subsequent resonant scattering of sunlight. As mentioned above, the resonance scattering emission vastly exceeds the direct auroral emission. The data, therefore, were predicted to reflect auroral precipitation at about 450 seconds (07:41:30 UTC) that would continue until the end of the flight. But, as noted in Hecht et al. (2019), the short-lived nature of some of the intense precipitation could affect some of the observations of the auroral emissions. In particular, the OI(630 nm) emission intensity was observed to be well below the model predictions. But emissions with short lifetimes (well

215 below a second) are not affected, and in fact some clear auroral signals are seen in the 391.4 nm observations. For example, between about 550 and 600 seconds (07:43:10-07:44:00 UTC) there are clear increases that correspond to the model predictions of increases in the 391.4 nm emission due to resonance scattering of N_2^+ ions.

However, the most noticeable aspect of the data is the sudden increase in signal just after 500 seconds (07:42:20 UTC) that continues, as a plateau, until a decrease just around 630 to 640 seconds (07:44:30-40 UTC). This is not reflected in the model

220 nor as shown in Hecht et al. (2019) in the greenline and redline data. Since the model does include sunlit N_2^+ this plateau is almost surely due to an excess of these ions above the rocket that begins after about 500 s when the rocket is descending below 400 km. This excess should be an indicator of some ion upflow, above the rocket, associated with the auroral precipitation
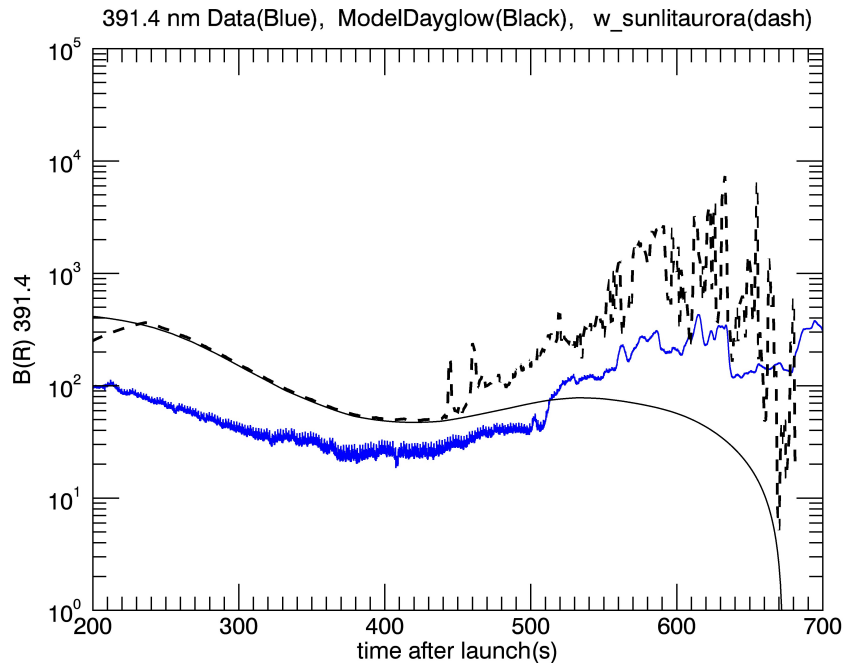
Figure 6. A plot of the brightness in Rayleighs of the emission from the $(0,0)$ band of the N_2^+ 1NG system at 391.4 nm from the RENU2 blue photometer vs time after launch. Also shown are the Strickland model predictions (see text) for the N_2^+ 1NG system at 391.4 nm dayglow (solid line) and for the N_2^+ 1NG system at 391.4 nm dayglow plus the N_2^+ 1NG system at 391.4 nm emission due to the auroral precipitation. A time after launch of 200 s corresponds to 07:37:30 UTC while 700 s corresponds to 07:45:40 UTC.

region, such has been discussed in other studies (Romick et al., 1999; Yau et al., 1993). The decrease at 630-640 seconds is probably due to a boundary associated with the end of the precipitation.

4.2 Correlation analysis

In order to investigate if the 427.8 nm emission corresponds to sunlit aurora, it is necessary to look at the emission altitude. For oxygen emissions, the altitudes are related to the energy of the precipitating electrons, resulting in expected altitudes of 100–120 km for 557.7 nm and 220–300 km for 630.0 nm (Omholt, 1971). The 427.8 nm emission is dependent on the availability of ionised nitrogen. From the model results in figure 5 one can infer that the nitrogen emissions would originate at lower altitudes. These would correspond to the altitude of the 557.7 nm emission or lower. This contrasts to sunlit aurora, where the expected emission altitude depends on which part is sunlit above 150 km. This corresponds to the altitude of the 630.0 nm emission. As all of these emissions originate from particle precipitation, one can correlate the emissions from these three lines, in an attempt to determine if the 427.8 nm emission is more correlated with the 557.7 nm or the 630.0 nm emissions.

The correlation will be performed using the MSP data, by calculating the Pearson's correlation coefficient (Edwards and
Penney, 1982) between the different wavelengths recorded in one scan. The coefficient is given by

$$\rho_{\lambda_1,\lambda_2}(t) = \frac{\text{cov}\left(C(\lambda_1,t), C(\lambda_2,t)\right)}{\sigma(\lambda_1,t)\sigma(\lambda_2,t)},$$

where cov is the covariance, σ the standard deviation and $C(\lambda,t)$ the meridian scan for a given wavelength, λ, and time, t. The
value of the correlation coefficient is limited between -1 and 1 inclusive, where 1 indicates that the $C(\lambda_1,t)$ and $C(\lambda_2,t)$ are
identically shaped and proportional to each other, and -1 indicates that they are $180°$ out of phase. A value of 0 indicates that
their relationship is completely random or $90°$ out of phase. The resulting correlation is independent of amplitude (normalised),
ensured by the standard deviation divisors in the equation. It is also symmetric, meaning that $\rho_{\lambda_1,\lambda_2} = \rho_{\lambda_2,\lambda_1}$.

Figure 7 shows the calculated correlation coefficients. In order to understand the coefficients, we first have to take into
consideration the dynamics and geometry of the MSP measurements. The different measured auroral emissions have sub-
stantially different emission lifetimes, with the shortest being the prompt emission of the 427.8 nm, which has a lifetime of
$5.38 \cdot 10^{-8}$ s (Itikawa et al., 1986). The other two are significantly slower at ≈ 0.7 s for the 557.7 nm emission and 110 s for the
630.0 nm emission. It is worth noting that ionospheric density changes and quenching could shorten these lifetimes somewhat.
Since the scan time for the MSP is 16 s, both the emissions at 427.8 nm and 557.7 nm will persist in only one scan. In the case
of the 630.0 nm emission, it will be visible over several scans, blending together recent emissions with previous emission, as
seen in figure 7. In relation to the correlation, this means that in most cases the correlation between the 630.0 nm emission and
the other two will be largest at the start of the auroral activity.

With respect to the calculation, there are some geometrical considerations to take into account. As the MSP scans from
magnetic north to magnetic south, a given angle off magnetic zenith will intersect different field lines depending on the altitude
one is looking at. This means that if an emission occurs on a given field line, the 630.0 nm emission from that field line will
end up in a different angular bin, compared to the 557.7 nm emission, due to the difference in emission altitude. This effect is
smallest close to zenith, and becomes larger as one moves away from zenith. Due to this change in angle, one would expect a
reduction in the correlation coefficient between these two emission, as the shape of the angular scan for the two emissions is
different.

Taking all of these considerations into account, it is now possible to start analysing the correlation coefficients in figure 7.
Firstly, it can be noted that the correlation between the red (630.0 nm) and the green (557.7 nm) emissions corresponds to
periods of strong auroral activity, showing correlation values larger than 0. At certain points in time the red-green correlation
is closely followed by the green-blue (427.8 nm), and the red-blue, for instance at 07:27 UTC, 07:36 UTC (120 s) and 07:44
UTC (600 s). One type of event that can generate this similarity is a period of high energy precipitation around magnetic zenith,
which causes emissions from the three lines within the same scan. These events are well known.

Looking at the correlation at 07:38 UTC (240 s) and 07:50 UTC (960 s) we have a situation where the red-blue correlation
is smaller than the green-blue. Taking into account the previously discussed mechanisms, the blue emissions occur at similar
altitudes to the green emissions. By following the correlation coefficients, it is possible to see that after two to three minutes
the difference in the correlation coefficient switches, with red-blue correlating more than green-blue. From the MSP data in
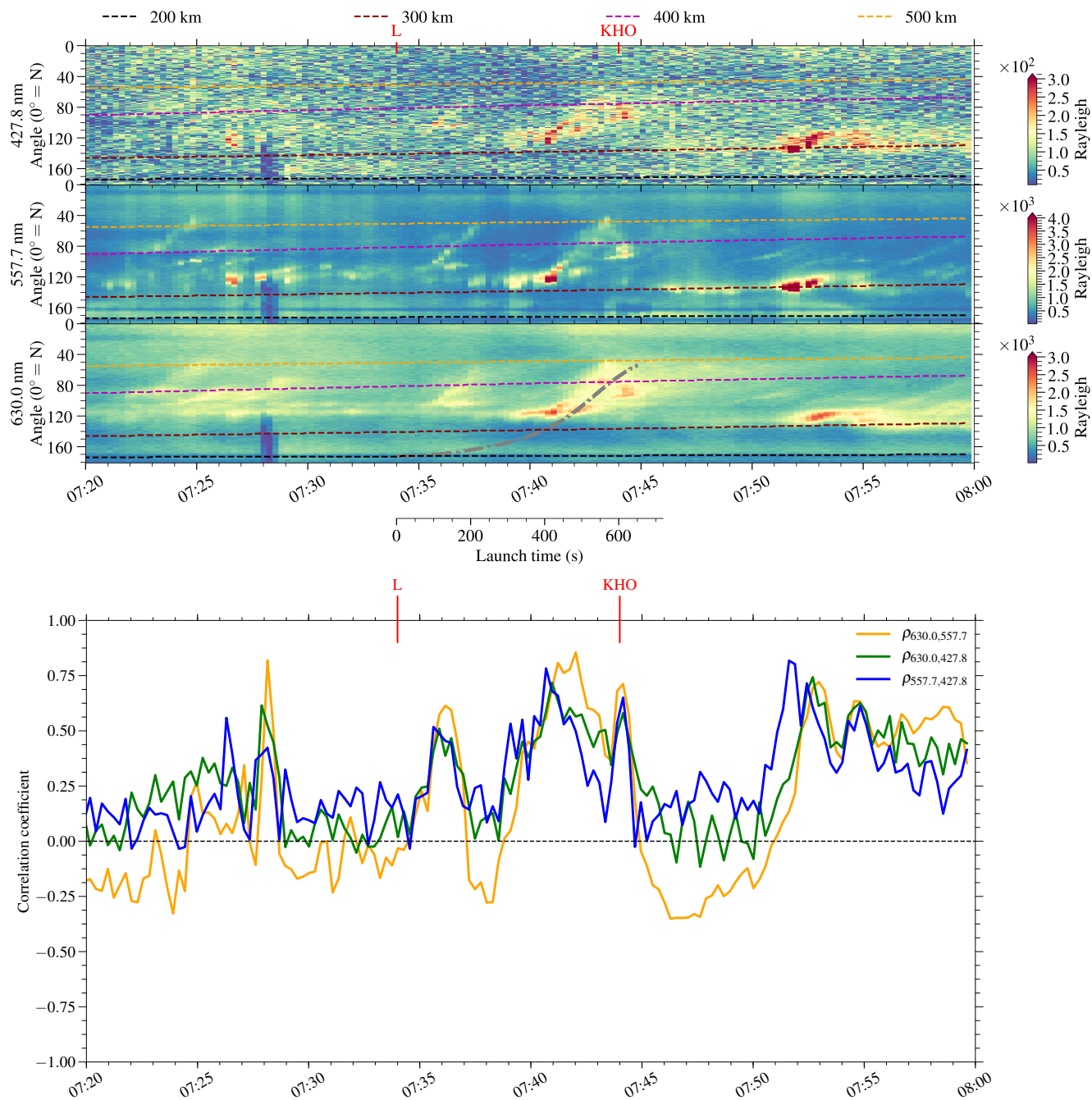
Figure 7. The top figure shows the MSP data just before and after the 07:34 UTC launch. The vertical blue stripe is due to clearing of snow from the slit. *L* and *KHO* mark the launch and passing east of KHO, respectively. Dashed lines represent the sunlit part of the atmosphere, with everything south of the line being sunlit at and above that altitude. Sunlit means that the light from the Sun has not passed below 150 km in order to get to the point of interaction. In the 630.0 nm figure the dashed and dotted gray line represents the rocket track mapped to the MSP field of view at a height of 240 km. The bottom figure shows the correlation coefficients for the time around the launch at 07:34 UTC based on the data in the top figure.

figure 7, we can see that if the emissions are from altitudes in the range 300–400 km, we can expect them to be sunlit. The sunlit altitude is displayed in the figure, calculated according to the method described in subsection 2.2. This observation of the time delay is consistent with the "cooking time" responsible for the observed ion upflow in the ionosphere (Lund et al., 2012). The ion upflow drags with it neutral molecules from lower altitudes, and would subsequently increase both the availability of N_2 and N_2^+ for the generation of sunlit aurora. An increase in available nitrogen was further confirmed by the observation of *in situ* 427.8 nm emission onboard the RENU2 rocket (Godbole et al., 2019). Together with the rate calculations in the previous section, we argue that a significant part of the observed 427.8 nm emissions can be attributed to sunlit aurora, which is further backed up by the observations made from the photometer onboard RENU2.

5 Conclusions

We have presented an optical study of the sunlit aurora present in the time around the RENU2 launch, 13 December 2015. Calculations of the possible EUV height show that the upper parts of the ionosphere above the Kjell Henriksen Observatory were sunlit at the time. An analysis using the correlation coefficient between three different wavelengths (427.8 nm, 557.7 nm and 630.0 nm) measured along the magnetic meridian at a given point in time was used to demonstrate the detection of sunlit aurora from ground-based instrumentation. By utilizing this correlation we show that the 427.8 nm emission occurs at the same heights as the 630.0 nm emissions. Using data from the RENU2 rocket and the estimated solar photon flux, it was found that sunlit aurora was a major part of the observed 391.4 nm and 427.8 nm emissions. The EUV photon flux and the electron flux were estimated to be $j_\gamma \approx 8.3 \cdot 10^{10}$ cm^{-2}s^{-1} and $j_e \approx 1.2 \cdot 10^{10}$ cm^{-2}s^{-1} respectively. Using these fluxes the ionisation rate of N_2^+ by photons was found to be $q_\gamma = j_\gamma \cdot \sigma_\gamma = 1.7 \cdot 10^{-6}$ s^{-1} and by electrons $q_e = j_e \cdot \sigma_e = 2.4 \cdot 10^{-6}$ s^{-1}. We have also shown that the correlation method presented here can be used to understand the altitude of the 427.8 nm emission as well as some of the processes occurring.

Author contributions. Article is primary written by Pål Gunnar Ellingsen with input from the other co-authors. Marc Lessard was additionally the RENU 2 PI.

Competing interests. The authors have no competing interests.

6 Acknowledgments

We acknowledge the Space Physics Data Facility(SPDF) and SPDF Contact: Natalia Papitashvili <Natalia.E.Papitashvili@nasa.gov> for the use of OMNI data which was downloaded from http://lasp.colorado.edu/home/eve/data/data-access/. RENU 2 data are available at NASA's Space Physics Data Facility, https://cdaweb.sci.gsfc.nasa.gov/index.html/. Supported by the Research Council of Norway/CoE under contract 223252/F50. Support was provided at the University of New Hampshire by NASA

ward NNX13AJ94G. JHH wishes to acknowledge support from NASA grant NNX13AJ93G. The data from the photometer plot can be found at http://mirl.sr.unh.edu/projects_renu2/FlightData/Hecht/

References

Abdou, W. A., Torr, D. G., Richards, P. G., Torr, M. R., and Breig, E. L.: Results of a comprehensive study of the photochemistry of N 2 + in the ionosphere, Journal of Geophysical Research, 89, 9069, https://doi.org/10.1029/JA089iA10p09069, 1984.

Brasseur, G.: Aeronomy of the middle atmosphere : chemistry and physics of the Stratosphere and Mesosphere, Atmospheric sciences library, Reidel, Dordrecht, 2nd rev. e edn., 1986.

Bug, M. U., Gargioni, E., Nettelbeck, H., Baek, W. Y., Hilgers, G., Rosenfeld, A. B., and Rabus, H.: Ionization cross section data of nitrogen, methane, and propane for light ions and electrons and their suitability for use in track structure simulations, Physical Review E - Statistical, Nonlinear, and Soft Matter Physics, 88, https://doi.org/10.1103/PhysRevE.88.043308, 2013.

Carlson, H. C., Spain, T., Aruliah, A., Skjaeveland, A., and Moen, J.: First-principles physics of cusp/polar cap thermospheric disturbances, Geophysical Research Letters, 39, 1–5, https://doi.org/10.1029/2012GL053034, 2012.

Chakrabarti, S.: Ground based spectroscopic studies of sunlit airglow and aurora, Journal of Atmospheric and Solar-Terrestrial Physics, 60, 1403–1423, https://doi.org/10.1016/S1364-6826(98)00060-1, 1998.

Chisham, G., Lester, M., Milan, S. E., Freeman, M. P., Bristow, W. A., Grocott, A., McWilliams, K. A., Ruohoniemi, J. M., Yeoman, T. K., Dyson, P. L., Greenwald, R. A., Kikuchi, T., Pinnock, M., Rash, J. P. S., Sato, N., Sofko, G. J., Villain, J. P., and Walker, A. D. M.: A decade of the Super Dual Auroral Radar Network (SuperDARN): Scientific achievements, new techniques and future directions, Surveys in Geophysics, 28, 33–109, https://doi.org/10.1007/s10712-007-9017-8, 2007.

Cohen, I. J., Lessard, M. R., Varney, R. H., Oksavik, K., Zettergren, M., and Lynch, K. A.: Ion upflow dependence on ionospheric density and solar photoionization, Journal of Geophysical Research A: Space Physics, 120, 10 039–10 052, https://doi.org/10.1002/2015JA021523, 2015.

Deehr, C., Sivjee, G., Egeland, A., Henriksen, K., Sandholt, P., Smith, R., Sweeney, P., Duncan, C., and Gilmer, J.: Ground-based observations of F region aurora associated with the magnetospheric cusp, Journal of Geophysical Research, 85, 2185, https://doi.org/10.1029/JA085iA05p02185, 1980.

Deng, Y., Fuller-Rowell, T. J., Ridley, A. J., Knipp, D., and Lopez, R. E.: Theoretical study: Influence of different energy sources on the cusp neutral density enhancement, Journal of Geophysical Research: Space Physics, 118, 2340–2349, https://doi.org/10.1002/jgra.50197, 2013.

Didkovsky, L., Judge, D., Wieman, S., Woods, T., and Jones, A.: EUV SpectroPhotometer (ESP) in Extreme Ultraviolet Variability Experiment (EVE): Algorithms and Calibrations, Solar Physics, 275, 179–205, https://doi.org/10.1007/s11207-009-9485-8, 2012.

Edwards, C. H. and Penney, D. E.: Elementary Linear Algebra, Prentice-Hall, 1982.

Fasel, G. J.: Dayside poleward moving auroral forms: A statistical study, Journal of Geophysical Research, 100, 11 891, https://doi.org/10.1029/95ja00854, 1995.

Godbole, N. H., Lynch, K. A., Lessard, M. R., Burleigh, M., Clausen, L., Clemmons, J., Fernandes, P. A., Fritz, B. A., Harrington, M., Hecht, J. H., Hysell, D., Kenward, D. R., Moen, J. I., Oksavik, K., Roberts, T. M., Sigernes, F., and Zettergren, M.: RENU2 Observations of Ion Upflow and Downflow, Geophysical Research Letters, under rev., 2019.

Greenwald, R. A., Baker, K. B., Dudeney, J. R., Pinnock, M., Jones, T. B., Thomas, E. C., Villain, J. P., Cerisier, J. C., Senior, C., Hanuise, C., Hunsucker, R. D., Sofko, G., Koehler, J., Nielsen, E., Pellinen, R., Walker, A. D., Sato, N., and Yamagishi, H.: DARN/SuperDARN - A global view of the dynamics of high-latitude convection, Space Science Reviews, 71, 761–796, https://doi.org/10.1007/BF00751350, 1995.

335   Hecht, J. H., Clemmons, J. H., Lessard, M. R., Kenward, D. L., Sadler, F. B., Fritz, B. A., Evans, J. S., and Lynch, K. A.: A New Technique for Estimating The Lifetime of Bursts of Electron Precipitation From Sounding Rocket Measurements, Geophysical Research Letters, https://doi.org/10.1029/2019gl082894, 2019.

Herlingshaw, K., Baddeley, L. J., Oksavik, K., Lorentzen, D. A., and Bland, E. C.: A Study of Automatically Detected Flow Channels in the Polar Cap Ionosphere, Journal of Geophysical Research: Space Physics, 124, 9430–9447, https://doi.org/10.1029/2019JA026916, 2019.

340   Hock, R. A., Chamberlin, P. C., Woods, T. N., Crotser, D., Eparvier, F. G., Woodraska, D. L., and Woods, E. C.: Extreme Ultraviolet Variability Experiment (EVE) Multiple EUV Grating Spectrographs (MEGS): Radiometric Calibrations and Results, Solar Physics, 275, 145–178, https://doi.org/10.1007/s11207-010-9520-9, 2012.

Hunten, D. M.: Sunlit aurora and the N2 + ion: A personal perspective, Planetary and Space Science, 51, 887–890, https://doi.org/10.1016/S0032-0633(03)00079-5, 2003.

345   Itikawa, Y., Hayashi, M., Ichimura, A., Onda, K., Sakimoto, K., Takayanagi, K., Nakamura, M., Nishimura, H., and Takayanagi, T.: Cross Sections for Collisions of Electrons and Photons with Nitrogen Molecules, Journal of Physical and Chemical Reference Data, 15, 985–1010, https://doi.org/10.1063/1.555762, 1986.

Johnsen, M. G., Lorentzen, D. A., Holmes, J. M., and Løvhaug, U. P.: A model based method for obtaining the open/closed field line boundary from the cusp auroral 6300 Å[OI] red line, Journal of Geophysical Research: Space Physics, 117, n/a–n/a,
350   https://doi.org/10.1029/2011JA016980, 2012.

Jokiaho, O., Lanchester, B. S., and Ivchenko, N.: Resonance scattering by auroral N2+: Steady state theory and observations from Svalbard, Annales Geophysicae, 27, 3465–3478, https://doi.org/10.5194/angeo-27-3465-2009, 2009.

Jokiaho, O.-P.: Spectral modelling of molecular nitrogen in aurora, Doctoral thesis, University of Southampton, http://eprints.soton.ac.uk/161195/, 2009.

355   Kenward, D. L., Lessard, M. R., Fritz, B. A., and Cohen, I. J.: Characterization of Soft Electron Precipitation in the Cusp Region during Poleward Moving Auroral Form Event, Geophysical Research Letters, under rev., 2019.

Lessard, M. R., Fritz, B., Sadler, B., Cohen, I., Kenward, D., Godbole, N., Clemmons, J. H., Hecht, J. H., Lynch, K. A., Harrington, M., Roberts, T. M., Hysell, D., Crowely, G., Sigernes, F., Syrjäsuo, M., Ellingson, P., Partamies, N., Moen, J., Clausen, L., Oksavik, K., Yeoman, T., Crowley, G., Sigernes, F., Syrj, M., Partamies, N., Moen, J., Clausen, L., and Oksavik, K.: Overview of the Rocket Experiment
360   for Neutral Upwelling Sounding Rocket 2 (RENU2), Geophysical Research Letters, accepted, https://doi.org/10.1029/2018GL081885, 2019.

Lorentzen, D. A., Kintner, P. M., Moen, J., Sigernes, F., Oksavik, K., Ogawa, Y., and Holmes, J.: Pulsating dayside aurora in relation to ion upflow events during a northward interplanetary magnetic field (IMF) dominated by a strongly negative IMF By, Journal of Geophysical Research: Space Physics, 112, 1–12, https://doi.org/10.1029/2006JA011757, 2007.

365   Lorentzen, D. A., Moen, J., Oksavik, K., Sigernes, F., Saito, Y., and Johnsen, M. G.: In situ measurement of a newly created polar cap patch, Journal of Geophysical Research: Space Physics, 115, 1–11, https://doi.org/10.1029/2010JA015710, 2010.

Lühr, H., Rother, M., Köhler, W., Ritter, P., and Grunwaldt, L.: Thermospheric up-welling in the cusp region: Evidence from CHAMP observations, Geophys. Res. Lett., 31, 6805, https://doi.org/10.1029/2003GL019314, 2004.

Lund, E. J., Lessard, M. R., Sigernes, F., Lorentzen, D. A., Oksavik, K., Kintner, P. M., Lynch, K. A., Huang, D. H., Zhang, B. C., Yang,
370   H. G., and Ogawa, Y.: Electron temperature in the cusp as measured with the SCIFER-2 sounding rocket, Journal of Geophysical Research: Space Physics, 117, https://doi.org/10.1029/2011JA017404, 2012.

Moen, J., Oksavik, K., and Carlson, H. C.: On the relationship between ion upflow events and cusp auroral transients, Geophysical Research Letters, 31, 1–5, https://doi.org/10.1029/2004GL020129, 2004.

Omholt, A.: The Optical Aurora, Sprinte-Verlag, https://archive.org/details/TheOpticalAurora, 1971.

375 Pesnell, W. D., Thompson, B. J., and Chamberlin, P. C.: The Solar Dynamics Observatory (SDO), Solar Physics, 275, 3–15, https://doi.org/10.1007/s11207-011-9841-3, 2012.

Picone, J. M., Hedin, A. E., Drob, D. P., and Aikin, A. C.: NRLMSISE-00 empirical model of the atmosphere: Statistical comparisons and scientific issues, Journal of Geophysical Research: Space Physics, 107, 1–16, https://doi.org/10.1029/2002JA009430, 2002.

Remick, K., Smith, R., and Lummerzheim, D.: The significance of resonant scatter in the measurement of N2+ first negative 0–1 emissions
380 during auroral activity, Journal of Atmospheric and Solar-Terrestrial Physics, 63, 295–308, https://doi.org/10.1016/S1364-6826(00)00233-9, 2001.

Romick, G. J., Yee, J. H., Morgan, M. F., Morrison, D., Paxton, L. J., and Meng, C. I.: Polar cap optical observations of topside (>900 km) molecular nitrogen ions, Geophysical Research Letters, 26, 1003–1006, https://doi.org/10.1029/1999GL900091, 1999.

Russell, C. T. and Elphic, R. C.: Initial ISEE magnetometer results: magnetopause observations, Space Science Reviews, 22, 681–715,
385 https://doi.org/10.1007/BF00212619, 1978.

Sadler, F. B., Lessard, M., Lund, E., Otto, A., and Lühr, H.: Auroral precipitation/ion upwelling as a driver of neutral density enhancement in the cusp, Journal of Atmospheric and Solar-Terrestrial Physics, 87-88, 82–90, https://doi.org/10.1016/j.jastp.2012.03.003, 2012.

Sandholt, P. E. and Farrugia, C. J.: Poleward moving auroral forms (PMAFs) revisited: responses of aurorae, plasma convection and Birkeland currents in the pre-and postnoon sectors under positive and negative IMF B y conditions, Ann. Geophys, 25, 1629–1652,
390 https://doi.org/10.5194/angeo-25-1629-2007, 2007.

Strickland, D., Bishop, J., Evans, J., Majeed, T., Shen, P., Cox, R., Link, R., and Huffman, R.: Atmospheric Ultraviolet Radiance Integrated Code (AURIC): theory, software architecture, inputs, and selected results, Journal of Quantitative Spectroscopy and Radiative Transfer, 62, 689–742, https://doi.org/10.1016/S0022-4073(98)00098-3, 1999.

Strickland, D. J., Daniell, R. E., Jasperse, J. R., and Basu, B.: Transport-Theoretic Model for the Electron-Proton-Hydrogen Atom Aurora,
395 2. Model Results, Journal of Geophysical Research, 98, 21 533–21 548, https://doi.org/10.1029/93JA01645, 1993.

Tabata, T., Shirai, T., Sataka, M., and Kubo, H.: Analytic cross sections for electron impact collisions with nitrogen molecules, Atomic Data and Nuclear Data Tables, 92, 375–406, https://doi.org/10.1016/j.adt.2006.02.002, 2006.

Woods, T. N., Eparvier, F. G., Hock, R., Jones, A. R., Woodraska, D., Judge, D., Didkovsky, L., Lean, J., Mariska, J., Warren, H., McMullin, D., Chamberlin, P., Berthiaume, G., Bailey, S., Fuller-Rowell, T., Sojka, J., Tobiska, W. K., and Viereck, R.: Extreme Ultraviolet Variability
400 Experiment (EVE) on the Solar Dynamics Observatory (SDO): Overview of Science Objectives, Instrument Design, Data Products, and Model Developments, Solar Physics, 275, 115–143, https://doi.org/10.1007/s11207-009-9487-6, 2012.

Yau, A. W., Whalen, B. A., Goodenough, C., Sagawa, E., and Mukai, T.: EXOS D (Akebono) observations of molecular NO + and N 2 + upflowing ions in the high-altitude auroral ionosphere , Journal of Geophysical Research, 98, 11 205, https://doi.org/10.1029/92ja02019, 1993.